PAPER

Check for updates

Synthesis of biocompatible gold nanoparticles for photothermal therapy by mineralization using peptides

Shuhei Yoshida, Koki Yoshida, Yoshiki Shitamukai, Makoto Ozaki, [ID]
Takaaki Tsuruoka [ID] and Kenji Usui [ID] *

Anisotropic gold nanostructures, such as rods and cubes, exhibit unique optical properties, including absorption in the near-infrared region, which makes them highly attractive for biomedical applications such as imaging and phototherapy. However, conventional synthesis methods often require toxic surfactants and strong reducing agents, limiting their biocompatibility. In this study, we developed a method for synthesizing biocompatible gold nanostructures suitable for photothermal therapy by mineralization using peptides. We designed peptides with different numbers of tryptophan (Trp) residues at N-terminal that can reduce gold ions and control nanoparticle growth. The peptides with fewer Trp residues were found to have a red-shifted maximum absorption wavelength at lower concentrations. A 2 : 1 ratio of gold ions to silver ions was optimal for the formation of anisotropic structures. The peptides successfully imparted high dispersibility to mineralized gold nanostructures. In addition, biocompatibility testing showed no toxicity in mineralized Au nanostructures. We studied the photothermal effect of visible light irradiation on the Au nanostructures, showing that they possessed high biotoxicity under light irradiation conditions. These results suggest that this method can be used for photothermal therapy. Our peptide-based approach offers a simple, safe, and biocompatible strategy to synthesize anisotropic gold nanostructures, which could be applied to the development of future nanomedical tools.

Introduction

Gold (Au) nanostructures have unique optical and catalytic properties.[1,2] Therefore, they are expected to have a wide range of applications in various fields such as engineering and biology.[3,4] Anisotropic Au nanostructures have several advantages over Au nanoparticles, including easier adjustment of surface plasmon resonance (SPR), high-efficiency photothermal effects, and high catalytic activity.[5–8] Notable examples of applications in the field of biotechnology include photothermal therapy using photothermal effects and bioimaging using chiroptical properties.[8–14] Anisotropic Au nanostructures are typically synthesized using template methods or seed-mediated growth methods, *e.g.*, Au seeds or silver (Ag) seeds. In the latter method, these of seeds are produced using high-concentration NaBH$_4$, and then Au ions are reduced to generate anisotropic Au nanostructures.[7,15–17] However, these conventional methods often use surfactants, which prevent the produced anisotropic Au nanostructures from agglomerating, and reducing agents, which can result in high biotoxicity.[18] Therefore, a method for synthesizing Au nanostructures with dispersibility and biocompatibility is necessary.

We focused on biomineralization to solve these problems. Biomineralization is a phenomenon in which organisms cleverly control the precipitation and reduction of inorganic substances.[19] For example, pearls from shellfish and animal bones and teeth are formed through biomineralization. It has been determined that proteins and peptides are responsible for this process. Peptides would be particularly useful for synthesizing biocompatible Au nanostructures for the following reasons. (1) Peptides would selectively reduce various metal ions depending on their amino acid sequences.[20–24] (2) Peptides would reduce Au ions without reducing agents, which are biotoxic and environmentally hazardous.[22,25,26] (3) After reducing Au ions, peptides would function as a dispersion stabilizer for Au nanoparticles.[27,28] Therefore, mineralization using peptides enables the fabrication of Au nanostructures with high biocompatibility and low environmental loading.

Although M. Tanaka *et al.* successfully synthesized Au nanoplates with absorption in the long-wavelength region by mineralization using peptides,[29] there are few reports of shapes other than plates being fabricated using peptides. It would be difficult to fabricate anisotropic Au nanostructures from only Au ion solutions using peptide-based mineralization.

Herein, we attempted to synthesize anisotropic Au nanostructures more easily using peptides with Ag ions than conventional peptide-mediated syntheses. Furthermore, we

Faculty of Frontiers of Innovative Research in Science and Technology (FIRST), Konan University, 6500047, Kobe, Japan. E-mail: kusui@konan-u.ac.jp; Tel: +81783031418

manufactured biocompatible Au nanostructures with photo-thermal effects by mineralization using peptides toward medicinal field.

Experimental

Materials

All chemicals and solvents were of reagent or high-performance liquid chromatography (HPLC) grade and used without further purification.

Synthesis of peptides

Peptides were manually synthesized by 9-fluorenylmethoxy-carbonyl (Fmoc)-based solid-phase peptide synthesis using Fmoc-NH-SAL-PEG resin (0.23 mmol g^{-1}, Watanabe Chemical Industries Ltd (Watanabe), Hiroshima, Japan). Peptide bonds were formed using 2-(1H-benzotriazole-1-yl)-1,1,3,3-tetramethyluronium hexafluorophosphate (HBTU, 10 eq., Watanabe) and 1-hydroxybenzotriazole monohydrate (HOBt, 10 eq., Watanabe) as a coupling reagent in the presence of Hunig's Base (N,N-diisopropylethylamine, DIEA, 15 eq., Watanabe) for 30 min at 37 °C. The Au^{3+} reducing peptide sequences were synthesized using Fmoc-amino acids (Watanabe). The side-chain-protecting groups used in this study were tert-butoxycarbonyl for tryptophan and lysine, 2,2,4,6,7-pentamethyl-2,3-dihydrobenzofuran-5-yl sulfonyl for arginine, and tert-butoxy for glutamic acid. After the synthesis, peptidyl resins were washed with chloroform 5 times and dried in vacuo. Cleavage from the resin and deprotection were performed by stirring with trifluoroacetic acid (TFA, Watanabe)/triisopropylsilane (FUJI-FILM Wako Pure Chemical Industries, Ltd (Wako), Osaka, Japan)/thioanisole (Wako)/MilliQ (Milli-Q Reference, Merck Ltd, Tokyo, Japan) (47/1/1/1, v/v/v/v) for 1 h. All the peptides were precipitated by the addition of cold diethyl ether, collected in 50 mL centrifuge tubes by centrifugation [3000 rpm, 5 min, 4 °C, CF18RS (Eppendorf Himac Technologies Co., Ltd, Ibaraki, Japan)] and dried in vacuo. Crude peptides were dissolved in 0.1% TFA in MilliQ water. The solutions were purified by HPLC [GL-7400 HPLC system (GL Sciences, Tokyo, Japan)] using an Inertsil ODS-3 column (10 × 250 mm; GL Science) with 0.1% TFA in MilliQ water (A solution) and 0.08% TFA in an acetonitrile (Kanto Chemical Co., Inc., Tokyo, Japan, B solution) gradient system, at a flow rate of 3.0 mL min^{-1}, detection at 220 nm. The respective purities were checked by HPLC [GL-7400 HPLC system (GL Sciences)] using an Inertsil ODS-3 column (4.6 × 150 mm; GL Science) with A solution and B solution gradient system, at a flow rate of 1.0 mL min^{-1}, detection at 220 nm. The peptides were analyzed using MALDI-TOF MS on an Axima Performance (Shimadzu Corporation (Shimadzu), Kyoto, Japan) mass spectrometer with sinapic acid as the matrix: W1, 1453.7 m/z ([M + H]$^+$ calcd. 1452.9); W2, 1639.8 m/z ([M + H]$^+$ calcd. 1634.0); W3, 1825.2 m/z ([M + H]$^+$ calcd. 1826.0); F1, 1414.2 m/z ([M + H]$^+$ calcd. 1413.9); and Nal1, 1464.2 m/z ([M + H]$^+$ 1463.9). In addition, the peptide purity and amino acid content of each peptide were evaluated by amino acid analysis using a COS-MOSIL 5C$_{18}$-AR-II column (4.6 × 250 mm; Nacalai Tesque, Inc.,

Kyoto, Japan) after samples were hydrolyzed in 6 M HCl at 110 °C for 24 h in a sealed tube and then labeled with phenyl isothiocyanate. The peptides were stored at 4 °C.

Gold mineralization using peptides or trisodium citrate

Peptides (25–100 μM) or trisodium citrate (25–100 μM) and HAuCl$_4$ (25–100 μM) were mixed in MilliQ water in a microtube and left to stand at the specified reaction temperature for 30 minutes, and then AgNO$_3$ (10–250 μM) was added. MilliQ water was added to bring the total volume to 350 μL. The mixture was then incubated at the specified temperature for 24 hours in an incubator (SI-300C, AS ONE Co., Osaka, Japan).

UV-vis measurements

The absorption peak derived from SPR on the sample after gold mineralization for 24 h was measured by a UV-1800 spectrometer (Shimadzu) using an eight-cell micromulticell (Shimadzu) with a 1 cm pathlength.

ζ-Potential measurements

5-Fold diluted sample solutions (750 μL for zeta-potential) were transferred into folded capillary cells DTS1070 (Malvern Instruments, Worcestershire, UK) for ζ-potential measurements. ζ-Potential data were acquired on a Zetasizer ZEN3600 instrument (Sysmex, Kobe, Japan) equipped with a 633 nm laser.

Dynamic light scattering (DLS) measurements

The sample solution (100 μL) was transferred into a UV transparent disposable cuvette (Sarstedt K.K., Tokyo, Japan), and DLS data were acquired on a Zetasizer ZEN3600 instrument equipped with a 633 nm laser.

Transmission electron microscopy (TEM) measurements

After Au mineralization, 20 μL samples were placed on TEM grids (Cu 200 mesh covered with a Nissin EM collodion membrane; Nissin-EM Co., Ltd, Tokyo, Japan). All samples were dried in vacuo prior to TEM measurements, which were conducted at an acceleration voltage of 120 kV (JEM-1400, JEOL Ltd, Tokyo, Japan).

Inductively coupled plasma-atomic emission spectroscopy (ICP-AES) measurements

The samples were pyrolyzed with 5 mL of (1 + 1) aqua regia and 5 mL of perchloric acid (HClO$_4$, Wako) for 1 h at 250 °C. After pyrolysis, the samples were dissolved in 2.5 mL of (1 + 1) aqua regia and 22.5 mL of MilliQ water. Calibration lines for each element were obtained using a gold standard solution (for Atomic Absorption Spectrochemical Analysis, Wako) in the range from 0 to 10 ppm. Au was detected at a wavelength of 242.795 nm using ICP-AES (SPECTROBLUERFMX36, Hitachi High-Tech Corporation, Tokyo, Japan).

Cell culture

Human cervical carcinoma (HeLa, Japanese Collection of Research Bioresources Cell Bank, Ibaraki, Japan) cells were cultured in Dulbecco's modified Eagle's medium (D-MEM, Wako) supplemented with 10% fetal bovine serum and 1% penicillin streptomycin. HeLa cells were seeded with 3.0×10^5 cells onto a Petri dish (Nest Biotechnology Co., Ltd, Wuxi, China) and cultured at 37 °C in a 5% CO_2 atmosphere for 24 h.

Cell viability measurements

HeLa cells were seeded with 5.0×10^4 cells in a 24-well plate (Thermo Fisher Scientific K.K., Tokyo, Japan) and cultured at 37 °C in a 5% CO_2 atmosphere for 24 h. 50 µL aliquots of mineralized Au nanostructure sample in D-MEM were added to 24-well plates and incubated at 37 °C in a 5% CO_2 atmosphere for 24 h. After incubation, the media were removed, and the cells were washed three times with 1× PBS. The cells were then treated with 200 µL of 0.25% trypsin at 37 °C in a 5% CO_2 atmosphere for 3 min. After adding 300 µL of the media, the cells were transferred into a microtube. The media were removed by centrifugation at 1500 rpm for 5 min (r. t.). Cells were suspended in 125 µL of 1× HEPES, and 50 µL aliquots were transferred into a 96-well plate. 1× HEPES (40 µL) and Cell Counting Kit-8 (CCK-8, 10 µL, DOJINDO LABORATORIES, Tokyo, Japan) were added to the cell suspensions which were kept at 37 °C in a 5% CO_2 atmosphere for 2 h. The UV signal was monitored at 450 nm using a UV spectrophotometer (MTP-310 Microplate Reader, Colona Electric, Ibaraki, Japan).

Cell death induction using photothermal effects caused by visible light irradiation

HeLa cells were seeded with 2.5×10^4 cells in a 96-well plate (Nest Biotechnology Co., Ltd) and cultured at 37 °C in a 5% CO_2 atmosphere for 24 h. 50 µL aliquots of 6-fold concentrated Au mineralized samples, which were prepared by centrifugation at 15 000 g for 1 h at 25 °C after transferring 300 µL of Au mineralized sample into a microtube, were added to 96-well plates, and HeLa cells were irradiated with visible light (>450 nm) for 30 min. After incubation, the media were removed, and the cells were washed three times with 1× PBS. 1× HEPES (90 µL) and CCK-8 (10 µL) were added to the cells which were kept at 37 °C in a 5% CO_2 atmosphere for 2 h. The UV signal was monitored at 450 nm using a MTP-310 Microplate Reader.

Results and discussion

First, we selected AuBP1 (W1), a peptide capable of reducing Au ions without the use of a reducing agent.[30] In order to compare differences in reducing ability, we designed and synthesized peptides W2 and W3 that have additional tryptophan (Trp) residues in their sequences (Fig. 1). Our previous studies showed that these peptides have different Au ion reducing abilities,[27] i.e., a higher number of Trp residues results in higher reducing ability of Au ions. It has also been shown that smaller spherical nanoparticles are formed as the number of Trp residues increases. Therefore, we investigated the effect of the

AuBP1 (W1)
H-W-A-G-A-K-R-L-V-L-R-R-E-NH₂

W2
H-W-W-A-G-A-K-R-L-V-L-R-R-E-NH₂

W3
H-W-W-W-A-G-A-K-R-L-V-L-R-R-E-NH₂

Fig. 1 Sequences of designed peptides in this study.

number of Trp residues on the reduction reaction under mixed conditions of Au and Ag ions. In addition, peptides (F1 and Nal1, Fig. S1) were designed by substituting the N-terminal amino acid (Trp) of W1 with phenylalanine (Phe) and naphthylalanine (Nal). These peptides were synthesized by the standard 9-fluorenylmethoxycarbonyl (Fmoc) solid phase peptide synthesis.[31] After purification by reverse phase HPLC, purity confirmation by HPLC and MALDI-TOF MS was performed (Fig. S2). The concentration was determined by amino acid analysis.

The resulting peptides were reacted with a mixture of $HAuCl_4$ solution (Au ions) and $AgNO_3$ solution (Ag ions) to synthesize Au nanostructures under conditions of [W1] = 50 µM, [$HAuCl_4$] = 100 µM, and [$AgNO_3$] = 50 µM for 24 h at 20 °C. The UV-vis spectra were compared with and without Ag ions. The addition of Ag ions caused a red shift in the SPR-derived maximum absorption wavelength of Au nanostructures, suggesting the formation of anisotropic Au nanostructures (Fig. S3a). TEM observations of the shapes of the Au nanostructures under Ag ion addition conditions revealed that non-spherical structures were formed (Fig. S3b). However, it was difficult to obtain aspect ratios from the structures obtained by TEM images. In addition, mineralization was performed by adding Ag ions and peptides. UV-vis measurements of the reaction solution after mineralization showed no absorption (Fig. S4a). Similarly, absorption was not observed even under conditions with only Au ions and Ag ions, without the peptides (Fig. S4b). These results indicate that Au nanostructures with SPR absorption in the long-wavelength region can be synthesized using Ag ions, Au ions, and Au ion-reducing peptides. Additionally, these results suggested that the peptide reduced Au ions but not Ag ions. Therefore, it was implied that Ag ions were involved in the crystal growth of the Au nanostructures.

In parallel, measurements were performed using [trisodium citrate] = 25–100 µM, [$HAuCl_4$] = 100 µM, and [$AgNO_3$] = 50 µM for 24 h at 20 °C. The UV-vis spectra showed a red shift at 25 µM trisodium citrate (Fig. S5). However, TEM observations showed that the shapes differed from that of the Au nanostructures prepared by mineralization using peptides (Fig. S6). Thus, trisodium citrate cannot form Au nanostructures with absorption in the long-wavelength region.

Next, we investigated the effects of the amino acid residue at the N-terminus in the peptides as well as the concentration of the peptides on the shape of the anisotropic Au nanostructures. The reaction was performed using W1, W2, W3, F1 and Nal1
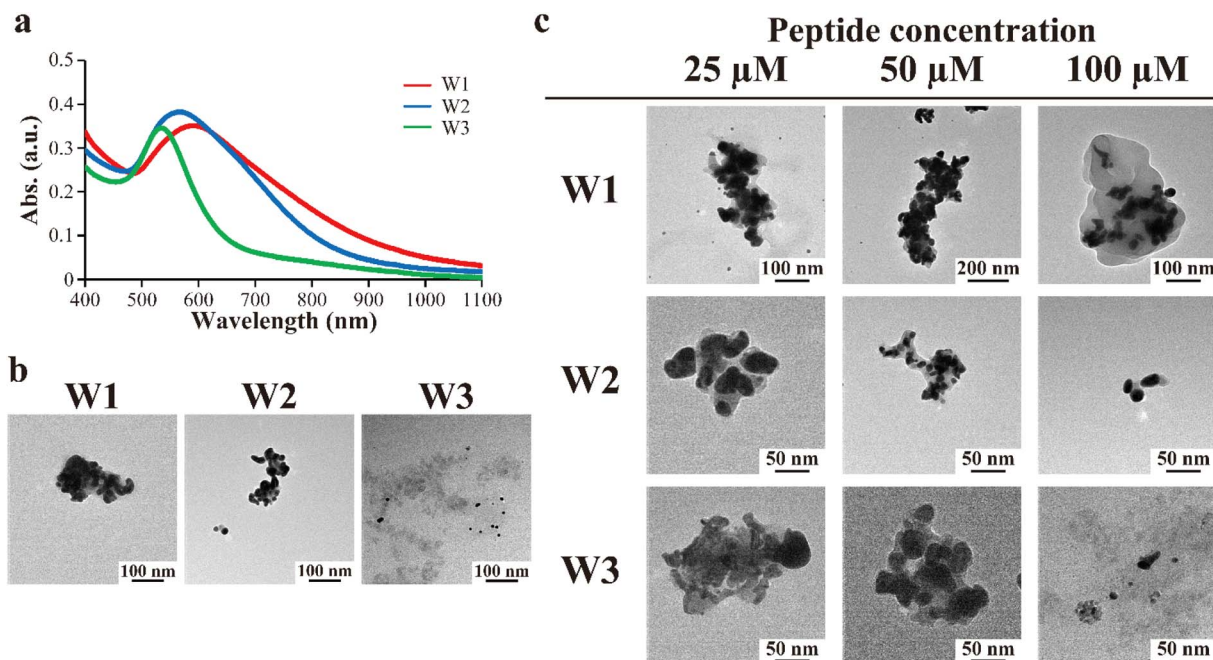
Fig. 2 (a) UV-vis spectra of samples after Au mineralization for 24 h using [Peptide] = 100 μM, [HAuCl$_4$] = 100 μM, and [AgNO$_3$] = 50 μM at 20 °C. (b) TEM images of samples after Au mineralization for 24 h using [Peptide] = 100 μM, [HAuCl$_4$] = 100 μM, and [AgNO$_3$] = 50 μM at 20 °C. (c) TEM images of samples after Au mineralization for 24 h using 25–100 μM of the peptides at 20 °C.

under conditions of [Peptide] = 100 μM, [HAuCl$_4$] = 100 μM, and [AgNO$_3$] = 50 μM for 24 h at 20 °C. After the reaction, UV-vis measurements and TEM observations were performed. In the case of W1, W2 and W3, UV-vis spectra showed that the fewer the Trp residues in the peptide sequence, the greater the red shift in the SPR-derived maximum absorption wavelength of the Au nanostructure (Fig. 2a). On the other hand, F1 showed no absorption originating from the Au nanostructures (Fig. S7a). Nal1 showed lower absorption than those of W1, W2 and W3 (Fig. S7b). These results suggested that Nal1 and F1 mineralized smaller amounts of Au nanostructures than W1, W2, and W3. Although the detailed reduction mechanism remains unclear, it has been reported that nitrogen atoms within amino acids coordinate with the gold(III) chloride ion ([AuCl$_4$]$^-$).[32] The Trp side chains in W1, W2, and W3 possess an indole nitrogen, whereas the Phe and Nal side chains in F1 and Nal1 lack nitrogen. Therefore, it was implied that the interaction between F1 and Nal1 with Au ions was weaker than W1, W2 and W3. As a result, the reduced amounts of Au ion using F1 and Nal1 would be less than W1, W2 and W3.

Next, the shape of the Au nanostructures produced was confirmed by TEM observations (Fig. 2b), showing that the anisotropy of Au nanostructures increases as the number of Trp residues decreases. These results suggested that the weaker the reduction ability of the peptide, the more anisotropic was the Au nanostructure formed. To determine the effect of the concentration of these peptides on the shape of the Au nanostructures, the reaction was carried out under the conditions of [W1] or [W2] or [W3] = 25–100 μM, [HAuCl$_4$] = 100 μM, and [AgNO$_3$] = 50 μM for 24 h, and UV-vis measurements and TEM observations were performed. The UV-vis spectra showed that the

maximum absorption wavelength red-shifted as the peptide concentration decreased (Fig. S8 and S9). TEM images showed that the lower peptide concentration generated higher anisotropy of the Au nanostructures (Fig. 2c and S10–12). Next, Dynamic Light Scattering (DLS) measurements were performed on these samples to investigate the particle size distribution of the Au nanostructures (Fig. S13). Except under [W1] = 25 and 100 μM, a bimodal size distribution was observed (Fig. S13a–c). This is thought to indicate the detection of both aggregates of Au nanostructures and individually dispersed particles. These results consisted with TEM images in Fig. 2c and S10–12. The amount of reduced Au ions was quantified by inductively coupled plasma-atomic emission spectroscopy (ICP-AES) measurements, revealing that the more Trp residues the peptide had, the greater the amount of Au ions were reduced (Fig. S14). These results (Fig. 2a and S14) suggested that Ag ions prefer to participate in the crystal growth of the Au nanostructure in conditions with the lower reducing peptides.

To evaluate the stability of the synthesized Au nanostructures, UV-vis measurements were performed on the samples two months after the reaction. The UV-vis spectra remained unchanged after one month (Fig. 3). The ζ-potential for the Au nanostructures immediately after mineralization and one month after mineralization was evaluated. The ζ-potential was 36.1 mV immediately after mineralization and 38.7 mV one week after mineralization. In parallel, the ζ-potentials for synthesized Au nanostructures using trisodium citrate were −20.5 mV at a trisodium citrate concentration of 25 μM, −33.4 mV at 50 μM, and −35.7 mV at 100 μM. The ζ-potential results showed that citric acid protects the surface of the Au nanostructures. These results suggest that peptides act as
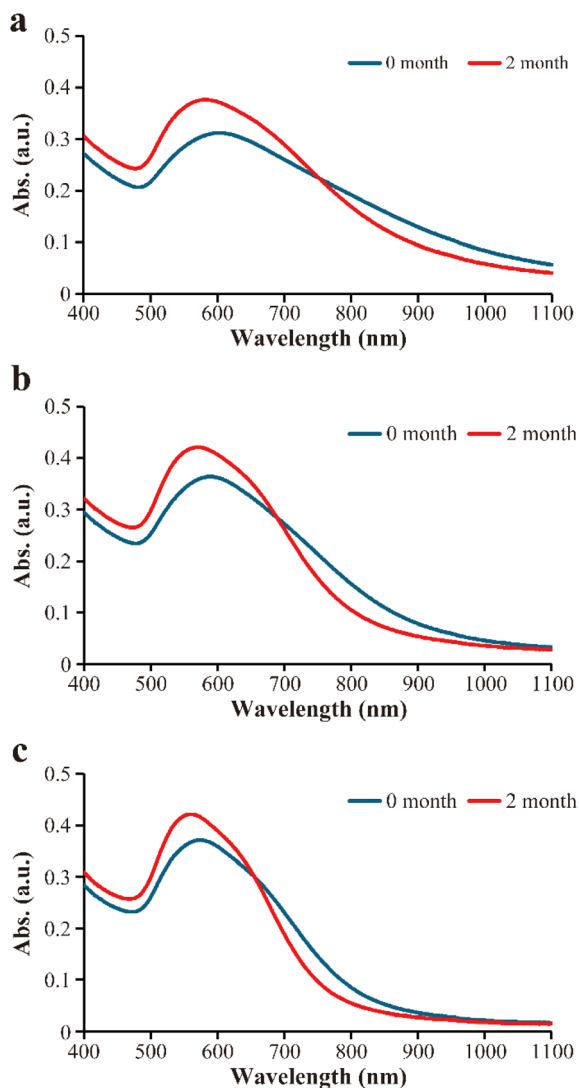
Fig. 3   UV-vis spectra of sample (Au nanostructures) immediately after mineralization and one month after mineralization using [Peptide] = 50 μM, [HAuCl$_4$] = 100 μM, [AgNO$_3$] = 50 μM for 24 h at 20 °C (a: W1; b: W2; c: W3).

dispersion stabilizers and that the dispersion could be maintained without protective agents such as surfactants. It is generally known that anisotropic Au nanostructures agglomerate and precipitate unless the surface of the structure is modified with a dispersion stabilizer.

The concentration of metal ions was changed, and UV-vis measurements and TEM observations of Au nanostructures were performed using 50 μM of W1, W2, and W3. With Au ion concentrations ranging from 25–100 μM, the maximum absorption wavelength of the UV-vis spectrum red-shifted as the Au ion concentration decreased (Fig. 4a–c). These results showed that Au nanostructures with long-wavelength absorption are formed when the concentration of Au ions is low. All Au nanostructures mineralized by W1 mineralization had a maximum absorption wavelength of 600 nm or more, and TEM observations showed that they formed Au nanoparticle

aggregates (Fig. S15). UV-vis measurements and TEM observations were performed at Ag ion concentrations ranging from 10–250 μM. The maximum absorption wavelength in the UV-vis spectrum was longest at 50 μM of Ag ion concentration (Fig. 4d–f). TEM observations showed that structures with absorption in the long-wavelength region are non-spherical (Fig. 4g). These results indicated that Au nanostructures with absorption at the longest wavelength could be synthesized under conditions where Au ions and Ag ions are present in a 2 : 1 ratio.

The effect of reaction temperature on the shape of the Au nanostructures was examined. Au nanostructures were synthesized at 10–30 °C under conditions of [W1] or [W2] or [W3] = 50 μM, [HAuCl$_4$] = 100 μM, and [AgNO$_3$] = 50 μM for 24 h. UV-vis, DLS measurements, and TEM observations were performed. The UV-vis results showed temperature-dependent changes in the spectra for W2 and W3 (Fig. 5a–c). There were two absorption wavelengths at 30 °C for W2 and at 25 °C and 30 °C for W3, suggesting the formation of anisotropic Au nanostructures. Under other temperature conditions, the spectra blue-shifted as the temperature decreased or increased. On the other hand, in the case of W1, no significant blue shift was observed, indicating that it is not easily affected by temperature. TEM observations showed that the Au nanostructures with two absorption wavelengths formed aggregates (Fig. S16). In addition, particle size was confirmed using DLS measurement. The particle size distribution similar to that observed in Fig. S13 was observed. (Fig. S17). These results suggested that there are optimal temperature conditions corresponding to the reducing ability of peptides in order to produce anisotropy in Au nanostructures.

Finally, we evaluated the cytotoxicity by adding these Au nanostructures to HeLa cells. Au nanostructures with the longest wavelength absorption were used. Specifically, the Au nanostructures were prepared by [W1] = 50 μM, [HAuCl$_4$] = 100 μM and [AgNO$_3$] = 50 μM for 24 h at 20 °C or [W2] or [W3] = 50 μM, [HAuCl$_4$] = 100 μM and [AgNO$_3$] = 50 μM for 24 h at 30 °C. The cell viability was evaluated 24 h after the addition of Au nanostructures. The peptide-mineralized Au nanostructures did not exhibit cytotoxicity (Fig. 6a). Furthermore, no cytotoxicity was observed under the three conditions where peptides with Au ions, or peptides with Ag ions were added (Fig. S18). We additionally evaluated cytotoxicity using commercially available Au nanorods. The commercially available Au nanorods were highly cytotoxic (Fig. 6a). The commercially available Au nanorods were protected on their surface by the surfactant hexadecyltrimethylammonium bromide (CTAB), which is thought to have caused the observed toxicity to cells. Therefore, the peptide-mineralized Au nanostructures were not only surface-protected by peptides but also showed low cytotoxicity. These results showed that the mineralized Au nanostructures produced by this method could be applied to photothermal therapy.

Furthermore, the photothermal effect of visible light (>450 nm) irradiation was evaluated using the same mineralized Au nanostructures as in the cytotoxicity evaluation. Here, we used a 10-fold concentrated peptide-mineralized Au nanostructure. It was shown that the viability of cells decreased with visible light
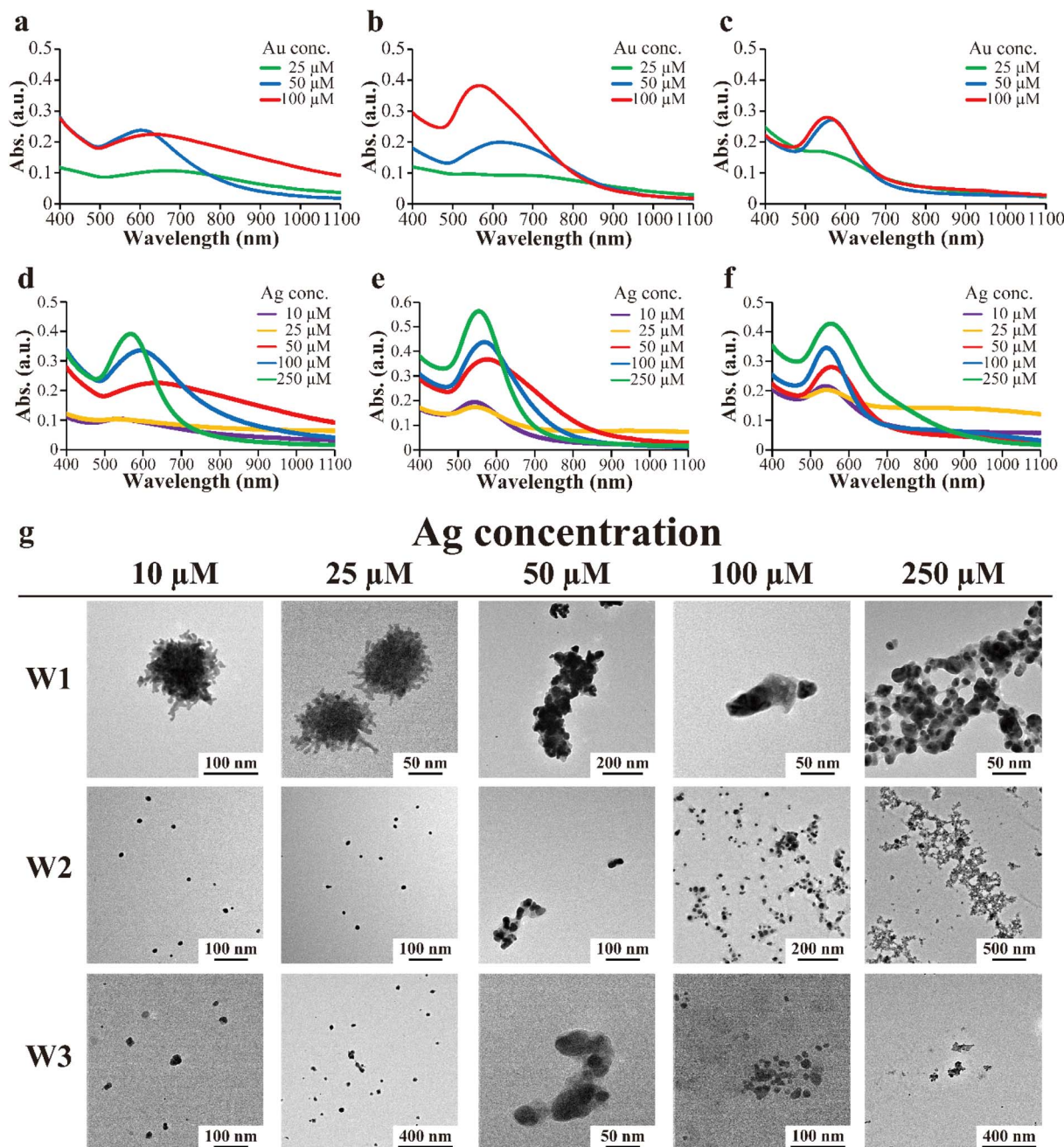
Fig. 4 (a–c) UV-vis spectra of samples after Au mineralization using various concentrations of Au ions (25–100 μM of HAuCl₄), [Peptide] = 50 μM, [AgNO₃] = 50 μM for 24 h at 20 °C (a: W1; b: W2; c: W3). (d–f) UV-vis spectra of samples after Au mineralization for 24 h using [Peptide] = 50 μM, [HAuCl₄] = 100 μM, [AgNO₃] = 10–250 μM at 20 °C (d: W1; e: W2; f: W3). (g) TEM images of samples after 24 h of Au mineralization using [Peptide] = 50 μM, [HAuCl₄] = 100 μM, [AgNO₃] = 10–250 μM at 20 °C.

irradiation in the presence of mineralized Au nanostructures (Fig. 6b). Furthermore, using only peptides, peptides with Au ions, and peptides with Ag ions, the photothermal effect was verified (Fig. S19). These results showed that Au nanostructures using peptide-based mineralization have a photothermal effect and could be applied to photothermal therapy. Under visible light irradiation conditions, the toxicity of Au nanostructures mineralized using W2 was the highest. This was due to their longer absorption wavelength compared to Au nanostructures

mineralized using W1. Under conditions where Au nanostructures were mineralized using W3, cell viability decreased even without light irradiation. This suggests that a large amount of Au nanostructures formed, leading to the expression of toxicity toward cells even within a short timeframe. Au and Ag ions could be reduced by mineralization using peptides to manufacture Au nanostructures with high dispersibility and biocompatibility.
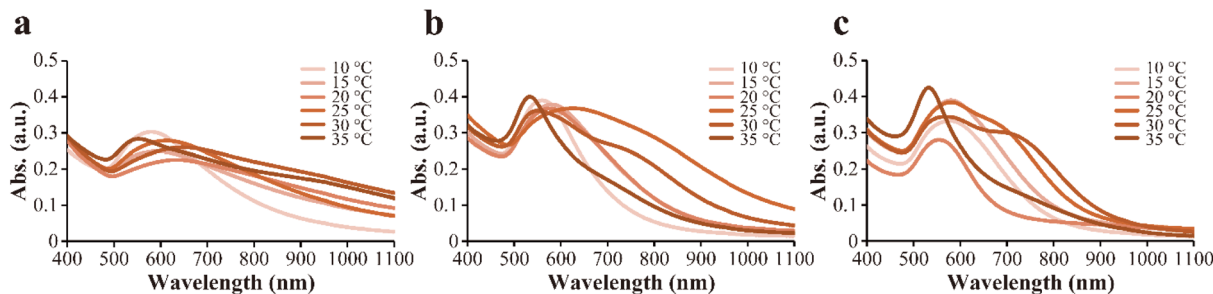
Fig. 5 (a–c) UV-vis spectra of samples after Au mineralization for 24 h using [Peptide] = 50 μM, [HAuCl₄] = 100 μM, [AgNO₃] = 50 μM at 10–35 °C (a: W1; b: W2; c: W3).
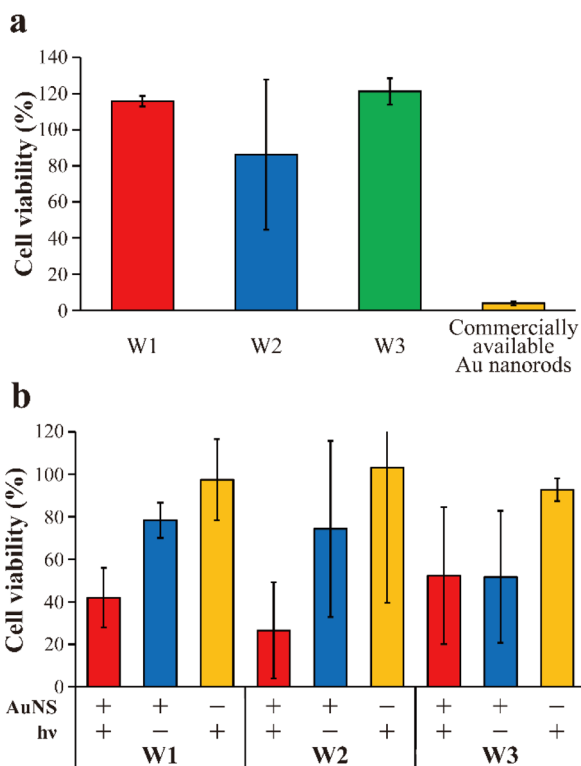

Fig. 6 (a) Cell viability after 24 hours with addition of mineralized Au nanostructures using peptides. The Au nanostructures were mineralized by [Peptide] = 50 μM, [HAuCl₄] = 100 μM and [AgNO₃] = 50 μM for 24 h. For W1, mineralization was performed at 20 °C, while for W2 and W3, it was performed at 30 °C. (b) Investigation of cell viability under conditions with or without addition of Au nanostructures and with or without light irradiation. The Au nanostructures were mineralized by [Peptide] = 50 μM, [HAuCl₄] = 100 μM and [AgNO₃] = 50 μM for 24 h. For W1, mineralization was performed at 20 °C, while for W2 and W3, it was performed at 30 °C.

Conclusions

In conclusion, we successfully manufactured biocompatible and highly dispersible Au nanostructures and achieved the expression of cytotoxicity upon light irradiation. In the manufacturing of Au nanostructures, the fewer the Trp residues in the sequence and the lower the peptide concentration, the easier it was to form Au nanostructures with long-wavelength absorption. In other words, these results showed that anisotropic Au nanostructures were

more easily formed under conditions where the reducing ability of the peptide was low and with a lower concentration of Au ions. However, it was suggested that the absorbance was low and the amount of Au nanostructures formed was small. The most anisotropic Au nanostructures were formed at 50 μM Ag ions with a 2 : 1 ratio of Au : Ag ions. When the reaction temperature was varied, 20 °C was found to be optimal for W1, while 30 °C was optimal for W2 and W3. On the other hand, the size uniformity of the mineralized Au nanostructures was low (Fig. 2c and S10–13). To fabricate Au nanostructures with more uniform properties for other purposes and/or applications, it is necessary to optimize peptide structure and/or conditions such as temperature. The mineralized Au nanostructures were shown to have no long-term cytotoxicity, but they exhibited toxicity to cells upon visible light irradiation. Thus, we established to easier synthesis of anisotropic Au nanostructures using peptides with Ag ions than conventional peptide mineralization. Furthermore, we have successfully manufactured biocompatible Au nanostructures with photothermal effects by mineralization using peptides. Future applications include photothermal therapy *in vivo* and the direct fabrication of Au nanostructures within cells.

Author contributions

Shuhei Yoshida: conceptualization, data curation, funding acquisition, investigation, project administration, visualization, writing – review & editing, writing – original draft preparation. Koki Yoshida: data curation, investigation, validation, visualization, writing – review & editing. Yoshiki Shitamukai: data curation, investigation, validation, visualization, writing – review & editing. Makoto Ozaki: conceptualization, investigation, writing – review & editing. Takaaki Tsuruoka: supervision, writing – review & editing. Kenji Usui: funding acquisition, supervision, writing – review & editing, writing – original draft preparation.

Conflicts of interest

There are no conflicts to declare.

Data availability

The data supporting this article have been included as part of the supplementary information (SI). Supplementary information is available. See DOI: https://doi.org/10.1039/d5ra08717a.

Acknowledgements

References

1 H. Chen, L. Shao, Q. Li and J. Wang, *Chem. Soc. Rev.*, 2013, **42**, 2679–2724.

2 A. S. Hashmi and G. J. Hutchings, *Angew. Chem., Int. Ed.*, 2006, **45**, 7896–7936.

3 J. A. Jackman, A. Rahim Ferhan and N. J. Cho, *Chem. Soc. Rev.*, 2017, **46**, 3615–3660.

4 H. Jans and Q. Huo, *Chem. Soc. Rev.*, 2012, **41**, 2849–2866.

5 X. Sun and D. Qin, *J. Mater. Chem. C*, 2015, **3**, 11833–11841.

6 X. Ye, C. Zheng, J. Chen, Y. Gao and C. B. Murray, *Nano Lett.*, 2013, **13**, 765–771.

7 E. Martinsson, M. M. Shahjamali, N. Large, N. Zaraee, Y. Zhou, G. C. Schatz, C. A. Mirkin and D. Aili, *Small*, 2016, **12**, 330–342.

8 V. Biju, *Chem. Soc. Rev.*, 2014, **43**, 744–764.

9 Y. Hang, A. Wang and N. Wu, *Chem. Soc. Rev.*, 2024, **53**, 2932–2971.

10 M. Hu, J. Chen, Z. Y. Li, L. Au, G. V. Hartland, X. Li, M. Marquez and Y. Xia, *Chem. Soc. Rev.*, 2006, **35**, 1084–1094.

11 Y. Liu, P. Bhattarai, Z. Dai and X. Chen, *Chem. Soc. Rev.*, 2019, **48**, 2053–2108.

12 E. C. Dreaden, A. M. Alkilany, X. Huang, C. J. Murphy and M. A. El-Sayed, *Chem. Soc. Rev.*, 2012, **41**, 2740–2779.

13 C. M. Cobley, J. Chen, E. C. Cho, L. V. Wang and Y. Xia, *Chem. Soc. Rev.*, 2011, **40**, 44–56.

14 X. Yang, M. Yang, B. Pang, M. Vara and Y. Xia, *Chem. Rev.*, 2015, **115**, 10410–10488.

15 J. Qiu, M. Xie, T. Wu, D. Qin and Y. Xia, *Chem. Sci.*, 2020, **11**, 12955–12973.

16 M. Z. Wei, T. S. Deng, Q. Zhang, Z. Cheng and S. Li, *ACS Omega*, 2021, **6**, 9188–9195.

17 S. E. Lohse, N. D. Burrows, L. Scarabelli, L. M. Liz-Marzán and C. J. Murphy, *Chem. Mater.*, 2013, **26**, 34–43.

18 N. Li, P. Zhao and D. Astruc, *Angew Chem. Int. Ed. Engl.*, 2014, **53**, 1756–1789.

19 L. C. Palmer, C. J. Newcomb, S. R. Kaltz, E. D. Spoerke and S. I. Stupp, *Chem. Rev.*, 2008, **108**, 4754–4783.

20 M. Ozaki, T. Imai, T. Tsuruoka, S. Sakashita, K.-y. Tomizaki and K. Usui, *Commun. Chem.*, 2021, **4**, 1.

21 K.-y. Tomizaki, S. Wakizaka, Y. Yamaguchi, A. Kobayashi and T. Imai, *Langmuir*, 2014, **30**, 846–856.

22 S. Yoshida, K.-y. Tomizaki and K. Usui, *Chem. Commun.*, 2023, **59**, 13239–13244.

23 C. L. Chen and N. L. Rosi, *Angew. Chem., Int. Ed.*, 2010, **49**, 1924–1942.

24 T. Hatanaka, A. Matsugami, T. Nonaka, H. Takagi, F. Hayashi, T. Tani and N. Ishida, *Nat. Commun.*, 2017, **8**, 15670.

25 M. Ozaki, S. Yoshida, T. Tsuruoka and K. Usui, *Chem. Commun.*, 2021, **57**, 725–728.

26 C. Pigliacelli, K. B. Sanjeeva, Nonappa, A. Pizzi, A. Gori, F. B. Bombelli and P. Metrangolo, *ACS Nano*, 2019, **13**, 2158–2166.

27 M. Ozaki, S. Yoshida, M. Oura, T. Tsuruoka and K. Usui, *RSC Adv.*, 2020, **10**, 40461–40466.

28 C. J. Munro and M. R. Knecht, *Langmuir*, 2017, **33**, 13757–13765.

29 M. Tanaka, M. Hayashi, L. Roach, Y. Kiriki, T. Kadonosono, T. Nomoto, N. Nishiyama, J. Choi, K. Critchley, S. D. Evans and M. Okochi, *Acta Biomater.*, 2021, **131**, 519–531.

30 C. J. Munro, Z. E. Hughes, T. R. Walsh and M. R. Knecht, *J. Phys. Chem. C*, 2016, **120**, 18917–18924.

31 C. W. Chan and P. D. White, *Fmoc Solid Phase Peptide Synthesis: A Practical Approach*, Oxford University Press, New York, 2000.

32 A. M. Figat, B. Bartosewicz, M. Liszewska, B. Budner, M. Norek and B. J. Jankiewicz, *Langmuir*, 2023, **39**, 8646–8657.